

# White-dwarf red-giant mergers, early-type R stars, J stars and lithium

Xianfei Zhang<sup>1\*</sup> and C. Simon Jeffery<sup>1,2†</sup>

<sup>1</sup>*Armagh Observatory, College Hill, Armagh BT61 9DG, UK*

<sup>2</sup>*School of Physics, Trinity College Dublin, Dublin 2, Ireland*

Accepted . Received ; in original form

## ABSTRACT

Early-type R stars and J stars are a special type of carbon star, having enhanced nitrogen ( $[N/Fe] \approx 0.5$ ), lithium, a low  $^{12}C/^{13}C$  ratio ( $< 15$ ) and no s-element enhancements. The merger of a helium white dwarf with a red giant is regarded to be a possible model for the origin of early-type R stars, but the details of nucleosynthesis are not clear. In this paper we investigate three possible channels for helium white-dwarf + red-giant mergers, and find that, amongst the three, only a high-mass helium white dwarf subducted into a low core-mass red giant can make an early-type R star. Nucleosynthesis of elements carbon, nitrogen, oxygen and lithium correspond well with the observations. Furthermore, we find that the J stars may represent a short and luminous stage in the evolution of an early-R star.

**Key words:** stars: abundance, stars: white dwarfs, stars: evolution, stars: chemically peculiar, binaries: close

## 1 INTRODUCTION

Carbon stars are characterized by  $C/O > 1$  in their atmospheres. They are generally classified as spectral types N, R and J. The N-type carbon stars are recognized as normal carbon stars in which carbon is enhanced by third dredge-up during the asymptotic giant-branch (AGB) phase. R-type carbon stars are further classified into two groups (Shane 1928): early-R (hot) and late-R (cool). Late-R stars are similar to normal carbon stars (N-type), and the s-element over abundance is possibly produced during the AGB phase (Zamora et al. 2009). Early-R stars are different from late-R stars; they have near solar metallicity and show enhanced nitrogen ( $[N/Fe] \sim 0.5$ ), a low  $^{12}C/^{13}C$  ratio ( $< 15$ ) and no s-element enhancement (Dominy 1984; Zamora et al. 2009). Also, the early-R stars are lithium-rich and none are found in binary systems. The J-type carbon stars are similar to early-R stars, but show a high luminosity, a smaller ratio of  $^{12}C/^{13}C$  and more lithium on the surface (Abia & Isern 2000). The surface composition of N-type and late-R carbon stars can be reproduced by low-mass AGB nucleosynthesis models (Zamora et al. 2009). But the origins of the early-R stars and J stars are not clear, especially the nucleosynthesis responsible for their surface chemistries. The fact that, except for the wide binary BD+02°4338, all early-R stars are single stars, encouraged Izzard et al. (2007) to argue for an

origin based on binary-star mergers, which was supported by binary-star population-synthesis calculations

According to Izzard et al. (2007), a possible evolution channel for early-R stars is for a helium white dwarf (He WD) to merge with a red giant-branch (RGB) star. As the helium white dwarf comes into contact with the expanding red giant, a common envelope forms. Assuming spiral-in occurs faster than the envelope can be ejected, the white dwarf will merge with the helium core of the giant. The final outcome will be a single star having a core comprising the sum of the helium white dwarf and the red-giant (RG) helium core surrounded by an H-rich mantle. Izzard et al. (2007) discuss the composition of the envelope, which seems to be able to reproduce an enriched carbon surface. However, Piersanti et al. (2010) point out that the enhancement of carbon depends on whether efficient helium burning occurs during the merger process. To analyze the details of the merger process, Piersanti et al. (2010) performed a three-dimensional smoothed-particle hydrodynamics (3D SPH) simulation and discussed the subsequent evolution. According to their calculation, no efficient helium burning occurred which would dredge up carbon-enriched material to the surface. However, some high-mass helium-white-dwarf merger channels, *i.e.* where the white dwarf mass is greater than  $0.2 M_{\odot}$ , were not studied by Piersanti et al. (2010).

In order to survey a wider range of models, we have simplified the SPH simulation into a 1D stellar evolution calculation. A detailed nucleosynthesis analysis is included. Our result shows that the merger of a high-mass helium

\* E-mail: xiz@arm.ac.uk

† E-mail: csj@arm.ac.uk

white dwarf with a red giant could be a possible evolution channel for early-R stars and J stars.

## 2 METHODS

To investigate evolution following the merger of two white dwarfs, Zhang & Jeffery (2012b) considered three sets of assumptions concerning the rate of accretion onto the more massive star, representing different distributions of fast and slow accretion. To simulate the merger of a helium white dwarf with a red giant, following the results of SPH simulations (Yoon et al. 2007; Lorén-Aguilar et al. 2009; Piersanti et al. 2010), we consider only the case of fast accretion (or a fast merger).

Numerical simulations of stellar evolution are carried out using the stellar-evolution code Modules for Experiments in Stellar Astrophysics (MESA version 4028) (Paxton et al. 2011). For our experiments, it is difficult to control the required final mass of the helium white dwarf from a full binary star evolution calculation. Thus, an artificial method is adopted. We start with a zero-age main-sequence star of mass  $2.0 M_{\odot}$  (metallicity  $Z = 0.02$ ) and evolve it until the helium core reaches the required mass. Then the hydrogen envelope is completely removed to produce a naked helium core, essentially a pre-WD model. This is achieved artificially in MESA by switching off the nucleosynthesis and applying a high mass-loss rate until the required model is obtained. These models cannot ignite central helium burning and evolve straight to the white-dwarf (WD) track, ending up with a luminosity  $\log L/L_{\odot} = -2$  (see Zhang & Jeffery (2012b) for details). Similarly, a model for the RG core is constructed in exactly the same way, except that we consider separately the cases where the RG core is either warm or cold. Here, a "warm" core represent a true model RG core which is only just degenerate (degeneracy parameter  $\eta \approx 3(0.2 M_{\odot}) - 10(0.3 M_{\odot})$ ), whilst a cold core is much more degenerate ( $\eta = 12(0.2 M_{\odot}) - 80(0.4 M_{\odot})$ ). Our models do not include rotation; all mixing is complete and driven by convection (no semi-convection, no thermohaline mixing, no diffusion). We separate the subsequent simulation into three steps.

**Step one:** merge the helium white dwarf with the helium core of the red giant. Following Yoon et al. (2007); Lorén-Aguilar et al. (2009) and Piersanti et al. (2010), a fast accretion rate of  $10^4 M_{\odot} \text{ yr}^{-1}$  is adopted, implying that the merger takes a few minutes.

**Step two:** Switch off time-dependent terms, including nucleosynthesis. Numerically, build up a hydrogen envelope on top of the merged helium core from step one. This is achieved by reversing the process used to remove the envelope, in this case by applying a negative mass-loss rate. The composition of the hydrogen envelope is defined to be identical to that of the RG progenitor. The structure of the post-merger model is thus a cool degenerate central helium core with a helium-rich hot shell surrounded by a hydrogen

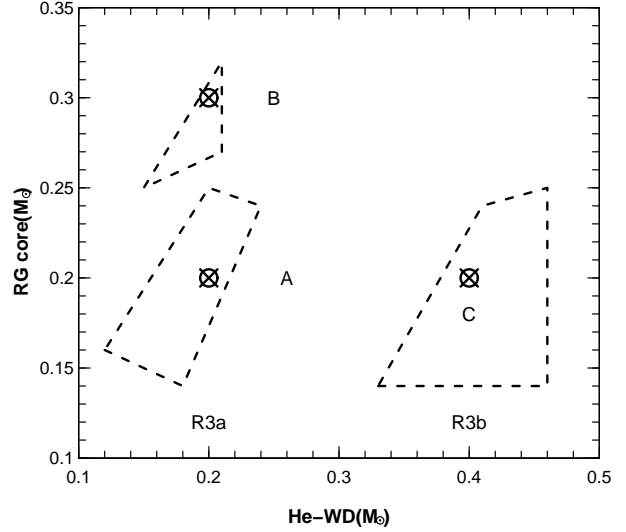


**Figure 1.** The circles with crosses shows the three types of model computed. Dashed lines indicate three zones defining possible evolution channels described by Izzard et al. (2007).

envelope.

**Step three:** Switch on time-dependent terms and evolve the post-merger model. Stop evolution before the thermally-pulsing AGB phase starts. No stellar winds were included in any of the calculations. The post-merger models are *defined* to have a final mass of  $2.0 M_{\odot}$ ; since the initial red giant has a mass of  $2.0 M_{\odot}$  to which is added the WD mass, we assume that a fraction of the total has been ejected during the common-envelope phase, but have chosen this fraction arbitrarily for the time being. One calculation with a final mass of  $1.5 M_{\odot}$  was made for comparison (§4.3.2).

## 3 MODELS

According to Izzard et al. (2007), there are two main WD-RG merger channels: low-mass He WD + RG (R3a) and high-mass He WD + RG (R3b). Channel R3a can be further divided into two groups: high core-mass RG and low core-mass RG. Thus, we set up three models for these three channels labelled Models A, B and C respectively (see Fig. 1 for details).

In the Piersanti et al. (2010) SPH simulations, all the models are low-mass He WD + low core-mass RG mergers, and all the accretion is by mass transfer from the helium white dwarf to the RG core. However, one concern is that the He WD has a higher density than the RG core. The massive He WD may therefore subduct (or sink) into the low-mass helium core. To cover these possibilities, we have considered two separate merger types; i) accretion from the He WD onto the helium core and ii) accretion from the helium core onto the He WD, i.e. the He WD subducts into the center

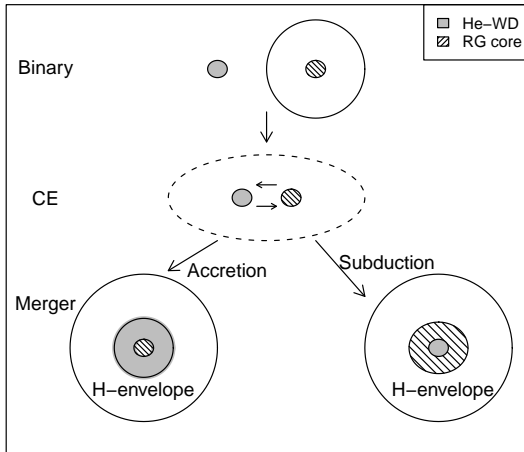


**Figure 2.** Cartoon illustrating two possible outcomes of a white-dwarf plus red-giant merger.

of helium core; see Table 1 and Fig. 2 for details. As noted above, the composition of the hydrogen envelope is taken from a  $2M_{\odot}$  RG model which has a  $0.2M_{\odot}$  helium core, and the final masses are  $2M_{\odot}$ .

#### 4 RESULTS AND DISCUSSION

In both "accretion" and "subduction" models, non-degenerate helium is effectively added to the surface of a degenerate helium core at a high rate. The combination of gravitational contraction and compression by the outer layers means that a hot shell develops at the WD/RG-core boundary, where the maximum temperature exceeds  $10^8 K$  (Fig. 3). Hydrogen burning starts from the helium/hydrogen boundary, where the released energy forces the star to expand to large radius (Fig. 4). The location of helium-ignition depends on the temperature and mass of the RG core and whether the WD is accreted or subducted. The merged stars are more luminous (or hotter) than normal red giants because of the larger core masses and, in some cases, an increased mean molecular weight in the envelope, due to dredge up of helium and carbon.

In the cases that both the WD and the RG core are cold, a helium-burning flame starts burning from the merger boundary inward to the center of the core (Fig. 3). As the helium-burning zone moves inwards, there follow a series of helium flashes, each subsequent flash decreasing in intensity, until the helium-burning shell (flame) reaches the center of the star. During the He-flash stages, luminosity first increases and then decreases. After the flame reaches the center of star, the star goes through a horizontal-branch or red-clump phase (core-helium plus shell-hydrogen burning). After core-helium exhaustion, a helium-burning shell

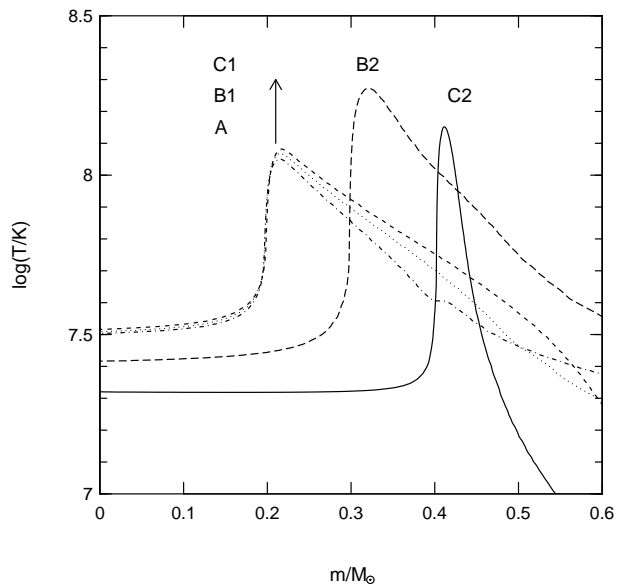


**Figure 3.** The temperature profile around temperature maximum for five models (labelled, see text and Table 1) just after merger. In these models both the RG core and the white dwarf are cold.

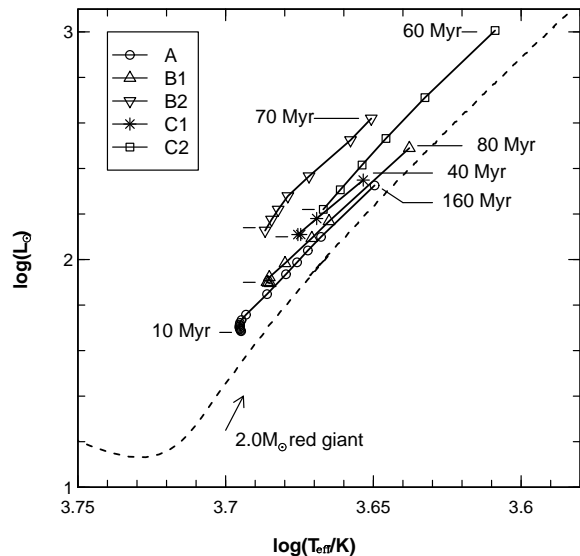


**Figure 4.** The evolutionary tracks of all models. The different symbols with solid lines indicate the major evolutionary stage for each model (evolution is always toward higher luminosity). Symbols are separated by intervals of  $10^7$  yrs. The first point on each track corresponds to  $10^7$  yrs after merger (marked by short horizontal ticks), the last is close to the start of the thermally-pulsing AGB; both can be identified in Figs. 6 (A), 7 (B1), 8 (B2), 11 (C1), and 12 (C2). The dashed line shows the evolutionary track of a normal  $2M_{\odot}$  star.

**Table 1.** Summary of the numerical experiments described in the text, showing the mass of the helium white dwarf, the core mass of the initial red giant, the assumed final mass of the merger product, and the type of white-dwarf-core interaction.

Models	WD mass ( $M_{\odot}$ )	Core mass ( $M_{\odot}$ )	Final mass ( $M_{\odot}$ )	Merger type
Model A	0.2	0.2	2.0	accretion/subduction
Model B1	0.2	0.3	2.0	subduction
Model B2	0.2	0.3	2.0	accretion
Model C1	0.4	0.2	2.0	accretion
Model C2	0.4	0.2	2.0	subduction

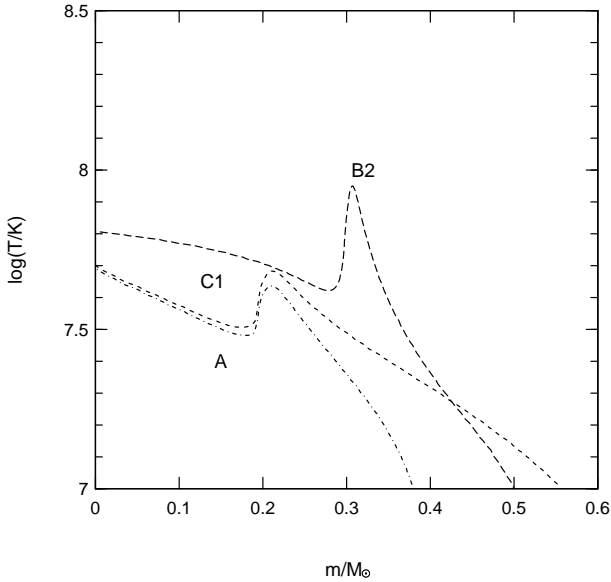


**Figure 5.** As Fig. 3, but for models where the RG core is warm and accretes a cold white dwarf.

will again form and evolution will be similar to the AGB double-shell burning phase.

Whilst our first calculations assumed a cold-degenerate model for the RG core, a more likely scenario is that the RG core should be *warm* at the time of merger (the core is heated by the hydrogen-burning shell). In practice, the pre-merger temperature of the accreted material is unimportant; fast accretion heats it to  $> 10^8$  K very quickly. Hence for models where the WD is subducted into the RG core (B1 and C2 below), the approximation is valid. In the remaining cases, we also computed models for accretion onto a warm RG core (Fig. 5), and report the result for each case below.

The majority of the test calculations do not show any change in the surface composition of the post-merger; where significant changes occur, we discuss the results in more detail.

#### 4.1 Model A: low-mass He WD + low-mass helium core

Immediately after merger, hydrogen burning drives a fully convective envelope, whilst helium burning is ignited at  $0.2 M_{\odot}$  (the RG-core boundary) and moves inwards (Fig. 6).  $^{12}\text{C}$  is produced by helium burning through the  $3\alpha$  reac-

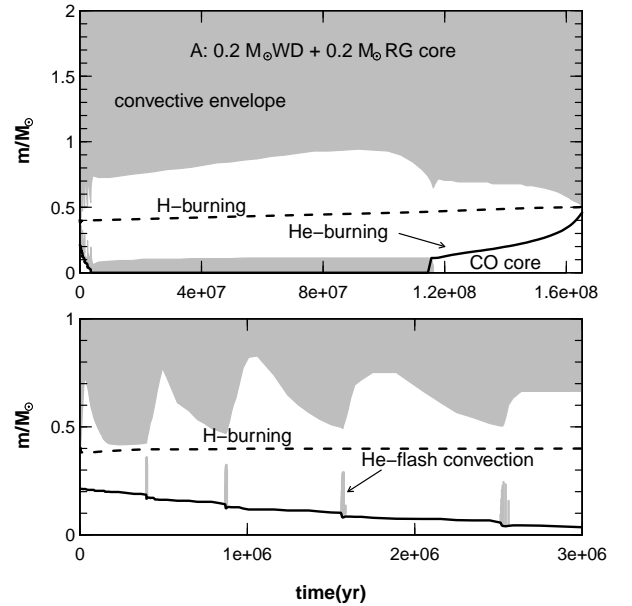


**Figure 6.** The convection structure of Model A, a  $0.2 M_{\odot}$  He WD accreted onto a  $0.2 M_{\odot}$  RG core. The grey area shows the convection zones, the dashed line shows the hydrogen burning front and the solid line shows the helium burning front. The bottom panel shows an enlargement around the phase of inward helium burning.

tion during the hot accretion phase. During the inward helium-burning phase, there is no flash-driven convection zone which can reach the hydrogen-rich envelope. Thus, no burning ash ( $^{12}\text{C}$ ) can be dredged up to the surface. In Fig. 6, the grey zone shows the convection zones, the dashed line shows the hydrogen-burning front and the solid line shows the helium burning front. Evolution takes  $1.66 \times 10^8$  yr from merger to the start of the thermally-pulsing double-shell burning AGB.

In the case of a WD accreted onto a *warm* RG core, helium ignition is nearly central, and more closely resembles the classical core-helium flash. There is no mixing of processed material to the surface.

These models confirm the Piersanti et al. (2010) conclusion that the merger of a low-mass He WD with a low-mass helium RG core cannot provide sufficient helium burning to bring  $^{12}\text{C}$  to the envelope.

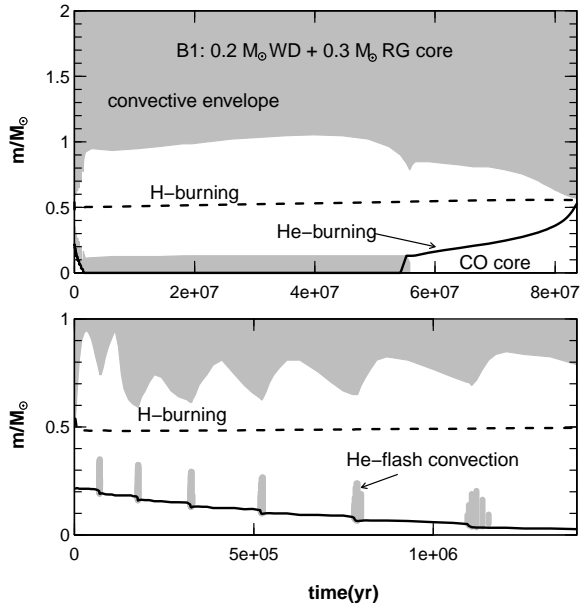


**Figure 7.** As Fig. 6, but showing the convection structure of Model B1, a  $0.2 M_{\odot}$  He WD subducted under a  $0.3 M_{\odot}$  RG core.

## 4.2 Model B: low-mass He WD + high-mass helium core

### 4.2.1 Model B1 (subduction)

Model B1 (Fig. 7) is similar to model A, and no flash-driven convection zone reaches the hydrogen envelope. Thus, the evolution is similar except for helium-core mass ( $0.5 M_{\odot}$  compared with  $0.4 M_{\odot}$  for case A) and evolution time ( $8.4 \times 10^7$  yr).

### 4.2.2 Model B2 (accretion)

Because  $0.3 M_{\odot}$  is effectively accreted, the helium shell in model B2 is much hotter than in model B1 (where only  $0.2 M_{\odot}$  is accreted), especially at the He/H boundary (Fig. 3). As a consequence, hydrogen-burning at the boundary is very strong and drives a convection zone which mixes hydrogen downwards into the helium shell, and also moves the hydrogen-burning shell downwards by  $\approx 0.1 M_{\odot}$  immediately after merger ( $t=0$  yr) (Fig. 8). This downwards mixing also dredges up CNO-cycled material which is mixed throughout the fully convective envelope, which thus becomes C-poor and N-rich. It takes  $7.6 \times 10^7$  yr from merger to the thermally-pulsing double-shell burning AGB.

There are some globular cluster stars which are C-poor and N-rich which have not yet been fully explained (Briley et al. 2002, 2004; Carretta et al. 2005; Cohen et al. 2005; Bekki et al. 2007). Our model may account for some of these stars. Model B2 produces stars with surface  $[C/Fe] = -1.15$ ,  $[N/Fe] = 0.88$  and  $[Na/Fe] = 1.42$ , which compares with observed abundances of  $[C/Fe]$ ,  $[N/Fe]$  and  $[Na/Fe]$  in the range of  $-0.5$  to  $0.5$ ,  $-1$  to  $2$  (Cohen et al. 2005; Bekki et al. 2007) (Fig. 9) and  $0.0$  to  $0.8$  (Yong et al. 2003; Bekki et al. 2007). Model B2 is also helium rich, with  $Y =$

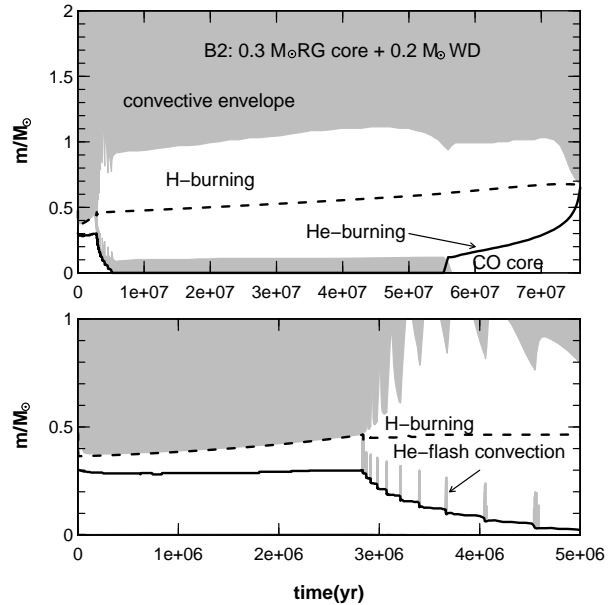


**Figure 8.** As Fig. 6, but showing the convection structure of Model B2, a  $0.2 M_{\odot}$  He WD accreted onto a  $0.3 M_{\odot}$  RG core.

$0.4$ ; some fraction of globular cluster stars have  $Y > 0.3$  (Bekki et al. 2007).

The oxygen abundance is in the range observed in globular clusters (*e.g.*  $[O/Fe] = -0.10$  in our model and  $-0.5$  to  $0.5$  in M15 (Cohen et al. 2005; Bekki et al. 2007)). However, our models are more C-poor than most C-poor globular-cluster stars, and also, our model produces lower-gravity and lower-temperature stars than observed in M15 (Fig. 10). However, we note that most of these cluster stars have lower metallicity than our models; it will be interesting to compute a low metallicity model in the future.

In the case of a WD accreted onto a *warm* RG core, helium ignition is in the same place (the WD / RG-core boundary) but, because the core is non-degenerate and the maximum temperature at the WD / RG-core boundary is *lower* than that in the cold-core model (Fig. 5), the shell flash is not strong enough to drive convection through the hydrogen shell, and there is *no* mixing of CNO-processed material to the surface.

## 4.3 Model C: high-mass He WD + low-mass helium core

### 4.3.1 Model C1 (accretion)

Model C1 (Fig. 11) is similar to Models A and B1 and, again, no flash-driven convection reaches the hydrogen envelope. Thus, evolution is similar except for a different core mass and evolution time ( $4.8 \times 10^7$  yr). The result for a WD accreted onto a *warm* RG core is also similar to that for case A, with no surface mixing.

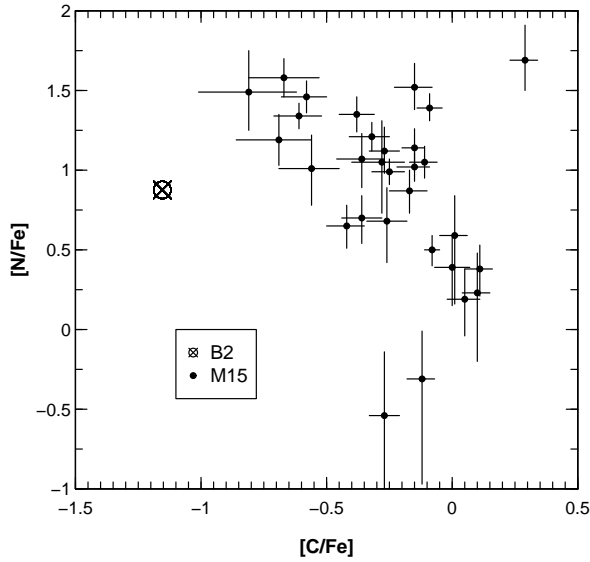


**Figure 9.**  $[C/Fe]$  vs.  $[N/Fe]$  ratios for Model B2 compared with the globular stars of M15 (filled circles) (Cohen et al. 2005; Bekki et al. 2007). The open circle with cross shows the model abundance of carbon and nitrogen during the major evolutionary stage.

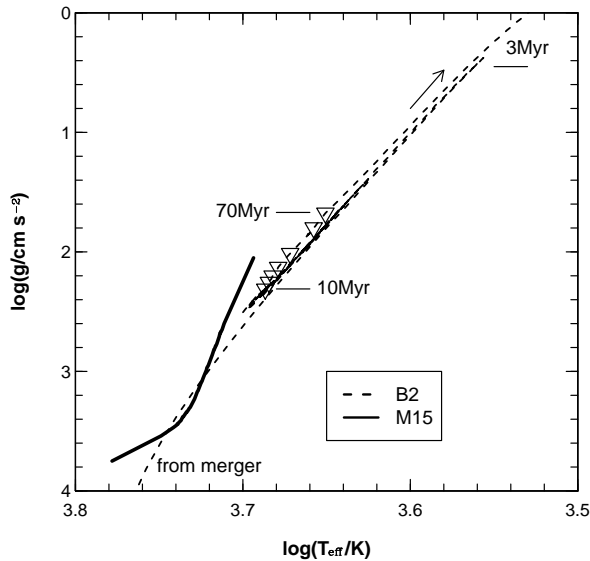


**Figure 10.** Gravity – temperature diagram showing the relation adopted for the globular stars of M15 by Cohen et al. (2005); Bekki et al. (2007) (thick solid line) and the evolutionary tracks for model B2 after merger (dashed line). The triangles denote intervals of  $10^7$  yrs during the major evolutionary stage (slow core-helium burning); other key times (since merger) are also indicated.

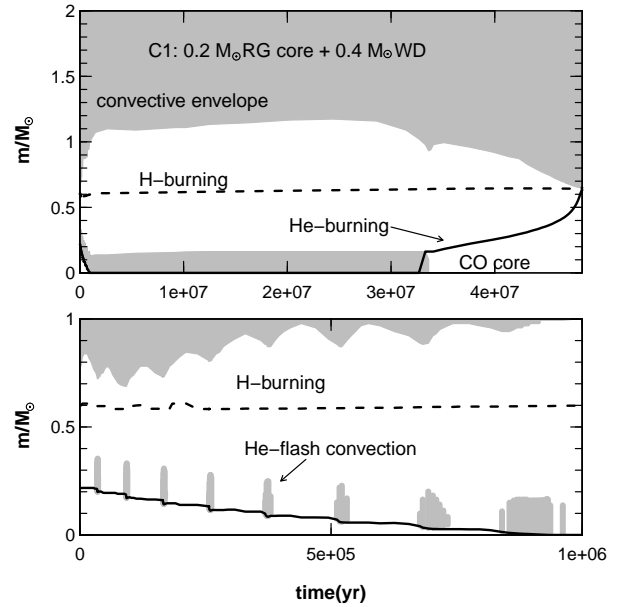


**Figure 11.** As Fig. 6, but showing the convection structure of Model C1, a  $0.4 M_{\odot}$  He WD accreted by a  $0.2 M_{\odot}$  RG core.

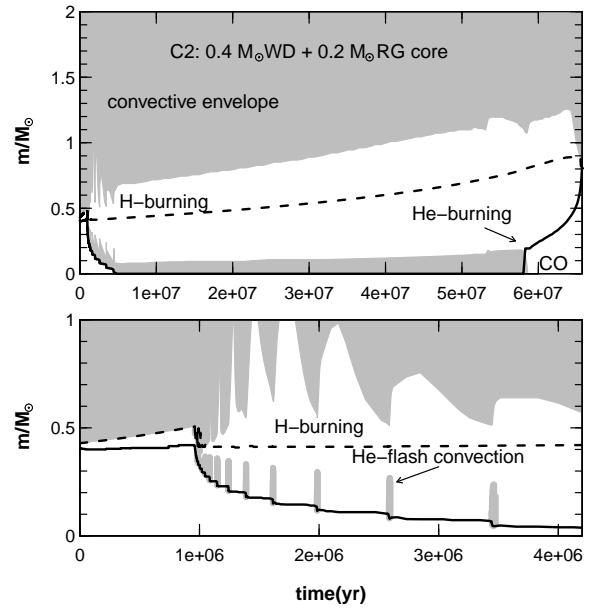


**Figure 12.** As Fig. 6, but showing the convection structure of Model C2, a  $0.4 M_{\odot}$  He WD subducted beneath a  $0.2 M_{\odot}$  RG core.

#### 4.3.2 Model C2 (subduction)

In model C2 (Fig. 12), the helium shell is very hot, and enhanced hydrogen-burning mixes  $\approx 0.2 M_{\odot}$  hydrogen into the helium shell. At the beginning of evolution, hydrogen burning forms a fully convective envelope, and forces the star to expand. Immediately following merger (and for approximately 150 years thereafter), the hydrogen-burning shell



converts available  $^{12}\text{C}$  to  $^{13}\text{C}$  and  $^{14}\text{N}$ , thus depleting  $^{12}\text{C}$  in the convective envelope and decreasing the  $^{12}\text{C}/^{13}\text{C}$  ratio by a factor of  $\approx 0.2$  (the  $^{12}\text{C}/^{13}\text{C}$  ratio in the envelope of the RGB progenitor is 26). Since the initial mixing is short-lived (50 years or four timesteps in our model), this factor is likely to be subject to several sources of uncertainty including the convection physics, numerics and the model parameters (*e.g.* masses and accretion rates).

After this, the hydrogen-burning shell detaches from the convection zone. Meanwhile, the core is relatively cold (20 MK), so the helium-burning shell is weak and relatively inactive ( $L_{\text{He}}/L_{\text{H}} \approx 10^{-6}$ ), whilst the hydrogen shell burns outwards through  $\approx 0.1 M_{\odot}$ . After  $10^6$  yr, the He-shell temperature rises sufficiently for a helium-shell flash to occur, driving a convection zone which mixes through to the hydrogen-rich envelope. Helium-burning continues in a series of flashes from the merger boundary to the center of the core.

During the first two helium-shell flashes, flash-driven convection connects the helium-burning shell to the convective envelope and dredges freshly-produced  $^{12}\text{C}$  ash from the helium-burning shell to the surface (the duration of these mixing events is short ( $< 200$  yr) so that insufficient  $^{12}\text{C}(p, \gamma)^{13}\text{N}(\beta^+ \mu)^{13}\text{C}(p, \gamma)^{14}\text{N}$  reactions occur as the carbon transits the H-shell to affect the surface  $^{13}\text{C}$  or  $^{14}\text{N}$  abundances directly). However, the events are long enough compared with the convective turnover time, assuming that this is comparable with a normal red-giant envelope, that the envelope will be fully mixed. The evolution of the structure is shown in Fig. 13 (lower panel), where the position of the H-burning shell is indicated by the maximum in nuclear energy production, which is very susceptible to local mixing events. Fig. 13 also shows the surface-abundance evolution of several species over the same interval (upper panel), demonstrating the dredge-up of  $^{12}\text{C}$  from  $3\alpha$  burning, enhanced  $^{14}\text{N}$  from CNO-cycle helium burning ( $[\text{N}/\text{Fe}] = 0.69$ ),  $^{22}\text{Ne}$  from  $\alpha$  captures on  $^{14}\text{N}$ , and the depletion of  $^{16}\text{O}$ , also associated with the CNO-cycle. The detailed evolution of the structures is likely to be sensitive to resolution and time step, as is the stability of the calculation; numerical problems with forced changes to the time step prevented further exploration.

The model takes  $6.6 \times 10^7$  yr to evolve from merger to the thermally-pulsing double-shell burning AGB; most of the time is spent as a red-clump star on the giant branch (squares in Fig. 14.)

Fig. 14 compares model C2 with 15 early-R stars from Zamora et al. (2009) on a  $g - T_{\text{eff}}$  diagram. The observed stars are satisfactorily close to the evolutionary tracks. However, since most of our models (and models of other giants) are almost coincident on such a diagram, this is more of a consistency check than a strong constraint. Fig. 15 compares the C/O ratios and  $^{12}\text{C}/^{13}\text{C}$  ratios for Model C2 with the early-R star measurements (Zamora et al. 2009). During the first million years after merger, the model evolves through the region occupied by early-R stars. The precise trajectory is subject to the uncertainty in the initial depletion of  $^{12}\text{C}$  discussed above, but the start and end points should be similar; it is conjectured that the allowable trajectory envelope should bracket the loci of observed early-R stars. The models generate a similar abundance of C and O to that observed. Furthermore, we find that  $^{22}\text{Ne}$  and  $^{23}\text{Na}$  are enriched to give  $[\text{Ne}/\text{Fe}] = 1.98$  ( $^{20}\text{Ne}/^{22}\text{Ne} = 0.17$ ) and

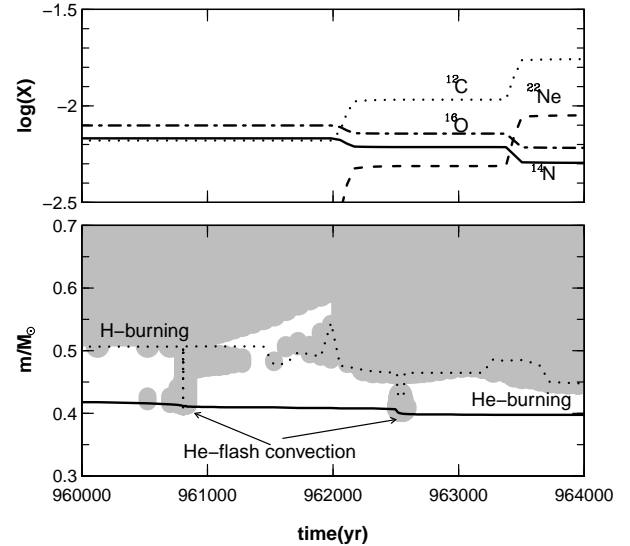


**Figure 13.** Bottom: as Fig. 12, but expanded around the the first two helium-shell flashes of Model C2. Top: the evolution of the surface abundance of  $^{12}\text{C}$ ,  $^{14}\text{N}$ ,  $^{16}\text{O}$  and  $^{22}\text{Ne}$  over the same interval.

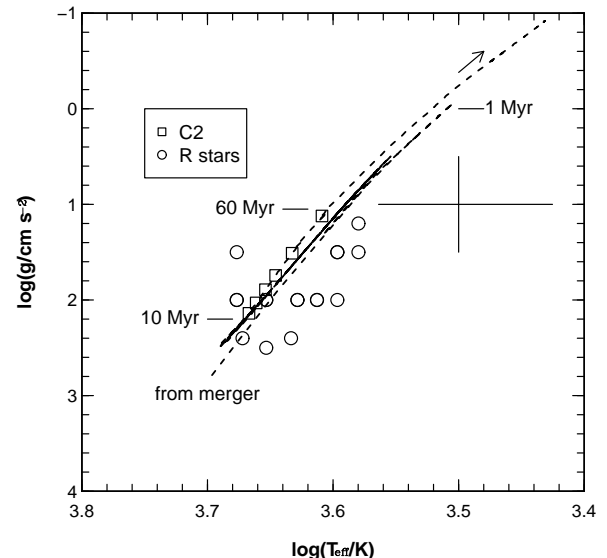


**Figure 14.** Gravity – temperature diagram showing the early-type R stars (circles) Zamora et al. (2009) and the evolutionary tracks for model C2 (dashed line). Squares denote intervals of  $10^7$  yrs during the major evolutionary stage. The cross shows the mean errors for the R-star measurements.

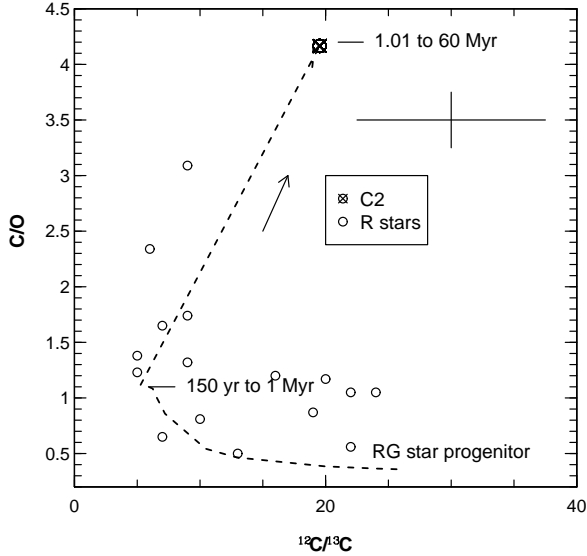


**Figure 15.** The post-merger evolution of the C/O and  $^{12}\text{C}/^{13}\text{C}$  ratios for Model C2 compared with the early-R stars of Zamora et al. (2009). The star HIP 58 786 has  $^{12}\text{C}/^{13}\text{C}=70$  and is not shown on this diagram. The dashed line shows the model evolution of C/O and  $^{12}\text{C}/^{13}\text{C}$  ratios after merger. The circle with cross shows the ratios of the C/O and  $^{12}\text{C}/^{13}\text{C}$  during most of this evolution. The cross shows the mean errors for the R-star measurements.

$[\text{Na}/\text{Fe}]=1.46$ . It is not known whether early-R stars are enriched in these species. Although the  $^{22}\text{Ne}(\alpha, n)^{25}\text{Mg}$  is a putative neutron source for further (s-process) nucleosynthesis (Cameron 1960), conditions in our models ( $T_{\text{max}} \approx 1.4 \times 10^8 \text{K}$  with  $\rho \approx 3.8 \times 10^3 \text{g/cm}^3$  in the helium shell) do not satisfy the necessary criteria ( $T > 2.2 - 3.5 \times 10^8 \text{K}$  and  $\rho > 1 - 3 \times 10^3 \text{g/cm}^3$ ) (Raiteri et al. 1991; Meyer 1994). Moreover, s-process nucleosynthesis is not included in the version of MESA used in these calculations.

For Model C2 with a final mass of  $1.5 M_{\odot}$  the evolutionary tracks are similar to those with a final mass of  $2.0 M_{\odot}$ , except that the final C/O ratio increases to 6.1 (instead of 4.2). This is because both models have the same core mass, and dredge up the same mass of carbon, which is consequently more concentrated in the lower-mass envelope.

#### 4.4 J stars and Lithium

Early-R and J stars have a notably large overabundance of lithium, which has so far been difficult to explain. To explain the overabundance of lithium in R CrB stars, Longland et al. (2012) showed that lithium can be produced by the merging of a helium white dwarf with a carbon-oxygen white dwarf if their chemical composition is rich in  $^3\text{He}$  from the previous evolution. Zhang & Jeffery (2012a) confirmed this in their He+He WD merger simulation. This model requires enough  $^3\text{He}$  to be left in the white dwarf after the end of main-sequence evolution and a hot enough zone to form during the merger. In our simulation, we obtained a mass fraction

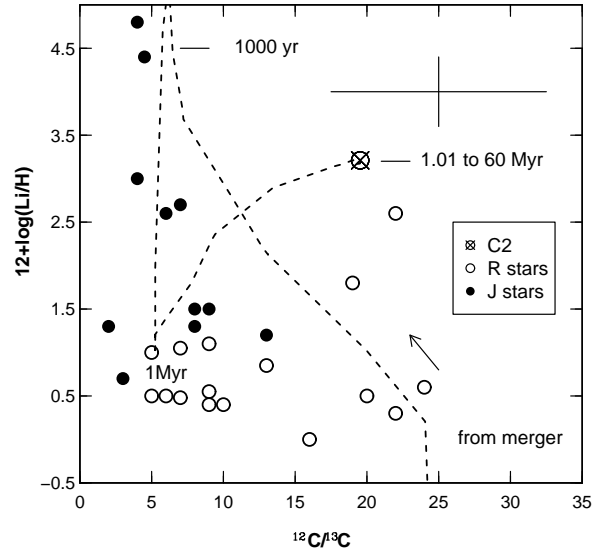


**Figure 16.** Lithium versus  $^{12}\text{C}/^{13}\text{C}$ . Circles show the early-R stars from Zamora et al. (2009). Dots show the J stars from Abia & Isern (2000). The dashed line shows the Li/H and  $^{12}\text{C}/^{13}\text{C}$  ratios during the evolution of model C2 immediately after merger. The circle with cross shows the Li/H and  $^{12}\text{C}/^{13}\text{C}$  ratios during the main core-helium burning phase. The cross shows the mean errors for the R-star measurements.

of  $5.6 \times 10^{-4}$   $^3\text{He}$  in the RG envelope before merger. We introduced this mass fraction into the envelope of the post-merger models. The hot He-burning shell drives convection which mixes  $^3\text{He}$  down into the He-burning shell where it burns with  $^4\text{He}$  to produce  $^7\text{Li}$  [ $^3\text{He}(\alpha, \gamma)^7\text{Be}(e^-, \nu)^7\text{Li}$ ].

For the new born  $^7\text{Li}$  to survive, the  $^7\text{Be}$  must be transferred to a cooler region rapidly before the decay occurs. Thus, in a manner similar to that described by Cameron & Fowler (1971), the  $^7\text{Li}$  may or may not appear on the surface depending on whether sufficient convection occurs (see Fig. 12). In our models, Models B2 and C2 both produce lithium. However, in Model B2 the newborn lithium is almost totally destroyed immediately by the reaction  $^7\text{Li}(p, ^4\text{He})^4\text{He}$ . In Model C2, the star retains its high lithium abundance because the mixing is very effective. While the star goes through its high-luminosity phase, its surface reaches a peak lithium abundance while the  $^{12}\text{C}/^{13}\text{C}$  ratio is still low (Fig. 16). Thus, J stars may represent just a special stage during the formation of early-R stars, as already hinted at by Abia & Isern (2000).

This stage, where  $^{12}\text{C}/^{13}\text{C}$  is very low, takes around 1 Myr, compared with 60 Myrs for the lifetime of Model C2. If C2 represents early-R stars, then J stars should constitute  $\approx 1/60$  of the total (Fig. 17).

Although the statistical evidence is not very strong, there are believed to be around 10 times more early-R stars than N stars (Blanco 1965). If the J stars constitute  $\approx 1/60$  of early-R stars, then the J:N ratio would be  $\approx 15\%$  which is the observed value (Abia & Isern 2000; Blanco 1965).



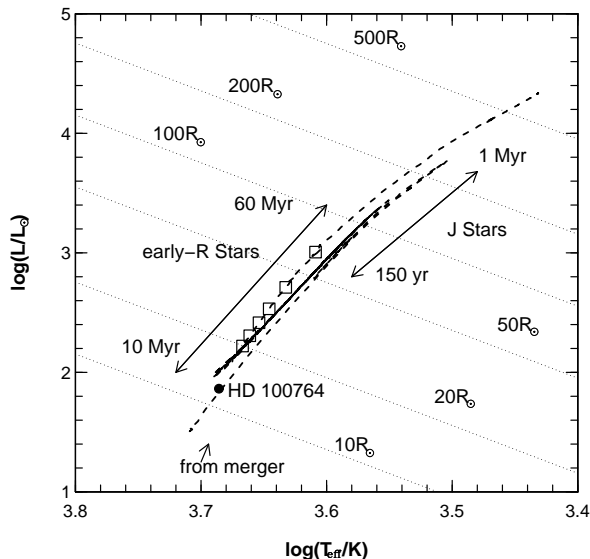


**Figure 17.** The evolutionary track of Model C2. Squares represent intervals of  $10^7$  yrs. The double-ended arrows show the luminosity ranges for model C2 over the time intervals indicated on the figure. These correspond approximately with the observed luminosity ranges of early-R and J stars. The dot shows HD 100764.

This argument assumes that J-stars, like early-R stars, are all single. This may not be true.

Approximately 10-15% of J stars are believed to have a silicate dust shell (Lloyd Evans 1991). Some consider such shells to be circumbinary disks. Although there is evidence for disk asymmetry, no J-star companion, or J-star orbit has so far been established (Deroo et al. 2007). If we consider the J-star phase of Model C2 to represent the immediate post-merger phase, it is possible that the observed silicate dust shell may form from the ejected part of the envelope. Since energy considerations demand that some fraction of the envelope should be ejected during merger, an asymmetric shell (or disk) would be an obvious geometry for the ejecta. If a silicate dust shell forms during merger and has a lifetime  $\approx 10^5$  years, then we might expect a fraction of 10-15% to show such shells, since the J stars are younger than the majority of early-R stars and have a lifetime of  $\approx 1$  Myr. We still need to explain why HD100764, an early-R star (Fig. 17), also shows a dust shell (Parthasarathy 1991; Sloan et al. 2007). However it has quite a low ratio of  $^{12}\text{C}/^{13}\text{C}=4$ , and shows emissions from polycyclic aromatic hydrocarbons (PAHs) (Sloan et al. 2007). We therefore suggest that HD100764 might be a very recent merger currently evolving *towards* the J-star phase.

## 5 CONCLUSION

Mergers of helium white dwarfs with red giants have been considered as a possible model for the origin of early-R stars. In this paper we have investigated three possible channels for He WD + RG mergers, and find that only a high-mass He

WD subducting into a low-core-mass RG star (Model C2) can produce early-R stars. However, nucleosynthesis of elements C, N, O, and Li for this model match the observations well. Moreover, J-stars may represent a short stage in this evolution. The fact that only Model C2 can produce early-R stars may explain why Izzard et al. (2007) produce ten times as many early-R stars as required. Our study shows that two of their proposed merger channels do not produce the correct surface composition. A more detailed population-synthesis study should be carried out to distinguish the boundaries of each of the evolution channels.

Our study has also shown that a low-mass He WD accreted onto a high-mass RG core may account for some C-poor and N-rich globular cluster stars. Lithium enrichment in red giants has previously been explained by one or more of rotational mixing, mass loss, planet accretion and deep circulation (Charbonnel & Balachandran 2000). In this paper we have shown that a He WD + RG merger may be an additional and important channel for producing lithium-rich red giants.

## ACKNOWLEDGMENTS

The Armagh Observatory is supported by a grant from the Northern Ireland Dept. of Culture Arts and Leisure.

## REFERENCES

- Abia C., Isern J., 2000, ApJ, 536, 438
- Bekki K., Campbell S. W., Lattanzio J. C., Norris J. E., 2007, MNRAS, 377, 335
- Blanco V. M., 1965, in Blaauw A., Schmidt M., eds, Galactic Structure Distribution and Motions of Late-Type Giants. p. 241
- Briley J. G., Briley M. M., Stetson P. B., 2002, AJ, 123, 2525
- Briley M. M., Harbeck D., Smith G. H., Grebel E. K., 2004, AJ, 127, 1588
- Cameron A. G. W., 1960, AJ, 65, 485
- Cameron A. G. W., Fowler W. A., 1971, ApJ, 164, 111
- Carretta E., Gratton R. G., Lucatello S., Bragaglia A., Bonifacio P., 2005, A&A, 433, 597
- Charbonnel C., Balachandran S. C., 2000, A&A, 359, 563
- Cohen J. G., Briley M. M., Stetson P. B., 2005, AJ, 130, 1177
- Deroo P., van Winckel H., Verhoelst T., Min M., Reyniers M., Waters L. B. F. M., 2007, A&A, 467, 1093
- Dominy J. F., 1984, ApJS, 55, 27
- Izzard R. G., Jeffery C. S., Lattanzio J., 2007, A&A, 470, 661
- Lloyd Evans T., 1991, MNRAS, 249, 409
- Longland R., Lorén-Aguilar P., José J., García-Berro E., Althaus L. G., 2012, ArXiv e-prints
- Lorén-Aguilar P., Isern J., García-Berro E., 2009, A&A, 500, 1193
- Meyer B. S., 1994, ARAA, 32, 153
- Parthasarathy M., 1991, A&A, 247, 429
- Paxton B., Bildsten L., Dotter A., Herwig F., Lesaffre P., Timmes F., 2011, ApJS, 192, 3

- Piersanti L., Cabezón R. M., Zamora O., Domínguez I., García-Senz D., Abia C., Straniero O., 2010, *A&A*, 522, A80
- Raiteri C. M., Busso M., Picchio G., Gallino R., Pulone L., 1991, *ApJ*, 367, 228
- Shane C. D., 1928, *Lick Observatory Bulletin*, 13, 123
- Sloan G. C., Jura M., Duley W. W., Kraemer K. E., Bernard-Salas J., Forrest W. J., Sargent B., Li A., Barry D. J., Bohac C. J., Watson D. M., Houck J. R., 2007, *ApJ*, 664, 1144
- Yong D., Grundahl F., Lambert D. L., Nissen P. E., Shetrone M. D., 2003, *A&A*, 402, 985
- Yoon S., Podsiadlowski P., Rosswog S., 2007, *MNRAS*, 380, 933
- Zamora O., Abia C., Plez B., Domínguez I., Cristallo S., 2009, *A&A*, 508, 909
- Zhang X., Jeffery C. S., 2012a, *MNRAS*, 426, L81
- Zhang X., Jeffery C. S., 2012b, *MNRAS*, 419, 452